Shape and Angle-of-Attack Measurements of Ram-Air Parachutes by Stereo Photogrammetry in the National Full-Scale Aerodynamics Complex

Edward T. Schairer,[1] James T. Heineck,[2] and Laura K. Kushner[3]
NASA Ames Research Center, Moffett Field, CA, 94035, USA

Kenneth J. Desabrais[4] and Keith Bergeron[5]
US Army, Combat Capabilities DEVCOM, Soldier Center, Natick, MA, 01760, USA

and
Justin M. Ellerbee[6]
US Air Force NFAC, Moffett Field, CA, 94035, USA

US Army MC-4/5 ram-air parachutes were tested in the 80- by 120-Ft test section of the National Full-Scale Aerodynamics Complex. Arrays of targets on the upper and lower surfaces of the central cell of the canopies were measured by stereo photogrammetry, and the target positions were used to estimate both the shape of the cell and angle of attack of the canopy. Forces and moments were measured by a six-axis load cell. Based on the photogrammetry and load-cell measurements, the relationships between lift, drag, and angle of attack were determined over a range of trailing-edge flap deflections, front riser lengths, and free-stream airspeeds. This paper describes the test, with an emphasis on the photogrammetry measurements, and presents a summary of results.

I. Nomenclature

c_x, c_y	=	camera horizontal, vertical scale factors (proportional to focal length)
D	=	drag
K_1, K_2	=	lens distortion correction factors
L	=	lift
m_{ij}	=	elements of 3x3 camera rotation matrix
V	=	free-stream velocity, kts
x	=	stream-wise distance downstream of the center of the Autonomous Guidance Unit (AGU), inches
y	=	lateral distance from test-section centerline, inches
z	=	vertical distance above floor of test section, inches
x_c, y_c, z_c	=	camera perspective center (stream-wise, lateral, vertical), inches
X, Y	=	horizontal, vertical image-plane coordinates (corrected for lens distortion), pixels
X_d, Y_d	=	measured horizontal, vertical image-plane coordinates (not corrected for lens distortion), pixels
X_P, Y_P	=	camera principal point, pixels
α	=	angle of attack (AoA), degrees
σ	=	standard deviation of least-squares solution

[1] Aerospace Engineer, Experimental Aero-Physics Branch (AOX).
[2] Physical Scientist, Experimental Aero-Physics Branch (AOX).
[3] Instrumentation Engineer, Wind Tunnel Systems Branch (AOI), AIAA Member.
[4] Research Aerospace Engineer, Aerial Delivery Directorate.
[5] Senior Research Aerospace Engineer, AIAA Associate Fellow.
[6] Test Engineer, National Full-Scale Aerodynamics Complex.

II. Introduction

In the spring of 2017, ram-air parachutes from the US Army Combat Capabilities Development Command Soldier Center (formerly called the US Army Natick Soldier Research, Development, and Engineering Center) were tested in the 80- by 120-Foot test section of the National Full-Scale Aerodynamic Complex (NFAC) at NASA Ames Research Center [1]. The purpose of this test was to create a database of basic aerodynamic performance data and data that can be used to validate computational fluid (CFD) and fluid-structure interaction codes. Other objectives were to investigate the effects on performance of fabric permeability, stress, and strain, which cannot be evaluated in drop tests. This test was expected to be the first of several wind-tunnel entries.

The test articles were the full-scale canopy sub-system of the US Army MC-4/5 ram-air free-fall personnel parachute system. These parachutes have been the primary ram-air personnel parachute system used by the US military for more than twenty years. Each canopy flew about 20 feet above the floor of the test section and was connected by suspension and control lines to an "autonomous guidance unit" (AGU) mounted on a platform just above the floor of the test section. The original test plan included a "variable trim platform" (VTP) between the canopy and the AGU. Together, the AGU and VTP would control of the angle of attack of the canopy. Important requirements of the test were to measure the angle of attack of the parachutes, the shapes of both the upper and lower surfaces of the central cell, and the orientation of the VTP. These measurements were made by the imaging group of the NASA Ames Experimental Aero-Physics Branch (Code AOX) using stereo photogrammetry.

Stereo photogrammetry allows the 3D coordinates of points in space to be computed from images of the points acquired by calibrated cameras from at least two directions. The camera calibrations express the transformation from 3D object space to the 2D image plane of each camera. Central issues in designing a photogrammetry system are: (1) the number and placement of cameras; (2) how the cameras are calibrated; and (3) how measurement points on the test article are defined. For 3D measurements, the cameras must be placed so that the angle between them is large enough to resolve displacements in the direction toward the baseline between them, where the optimum angle is 90°. Camera calibration is usually based on a full or simplified form of the collinearity equations [2], which treat the cameras as pinhole projections. Calibration coefficients are usually determined by imaging a set of targets whose spatial coordinates are known. Measurement points are usually defined by targets applied to the test article.

Photogrammetry has been applied in previous wind-tunnel tests of parafoils and parachutes. In 1991, Meyn and Bennett [3] measured the angle of attack of a parafoil in the NFAC 80- by 120-Ft test section using a stereo pair of upward-looking cameras mounted below the parafoil on the floor of the test section. The cameras were calibrated by suspending ropes from the ceiling with Styrofoam balls spaced at known intervals. Measurement points were defined by large rectangular patches sewn to the canopies. The photogrammetry was based on "line-of-sight" projection and did not account for lens distortion. In 1997, Matos et al. used a four-camera photogrammetry system to measure the angle of attack and shape of the upper surface of a parafoil suspended, inverted, from the ceiling of the 9- by 7-Ft wind tunnel at Georgia Institute of Technology [4]. Like Meyn and Bennett, they used a line-of-sight projection and calibrated their cameras by suspending balls from the ceiling of the test section. Measurement points were defined by a coarse grid marked on the canopy.

More recently, photogrammetry has been used by several of the present authors to measure the motions of conventional (circular) parachutes as they flew horizontally in the 80- by 120-Ft test section of the NFAC [5]. Cameras were mounted on the floor of the diffuser near opposite sidewalls and were pointed upstream. The cameras were calibrated by placing targets on a huge gantry crane that, when rolled into the test section, occupied much of the same space as the inflated parachutes. The spatial coordinates of the calibration targets were measured using a commercial photogrammetry system (V-STARS, [6]). Calibrations were based on the Direct Linear Transformation (DLT), which is a simplified form of the collinearity equations and can be used if the calibration targets are not coplanar [7]. Retro-reflective targets were sewn in a ring around the vent of each parachute and were illuminated by high-intensity lamps located next to each camera.

For the present test, three photogrammetry systems were deployed: one each to measure the upper and lower surfaces of the canopies, and a third to measure the orientation of the VTP. These systems were significantly different than the photogrammetry systems we used in previous tests. This paper describes all three systems, pointing out these differences, and presents typical results of the measurements.

III. Wind Tunnel

The tests were conducted in the 80- by 120-Ft test section of the National Full-Scale Aerodynamics Complex (NFAC) operated by the Air Force Arnold Engineering Development Complex (AEDC) at NASA Ames Research Center (Fig. 1, [8]). This indraft facility is the largest wind tunnel in the world. With an acoustic lining, the test section is 79 feet high, 119 feet wide, and approximately 190 feet long. Airspeeds in the test section up to 100 kts are produced

Fig. 1 National Full-Scale Aerodynamics Complex.

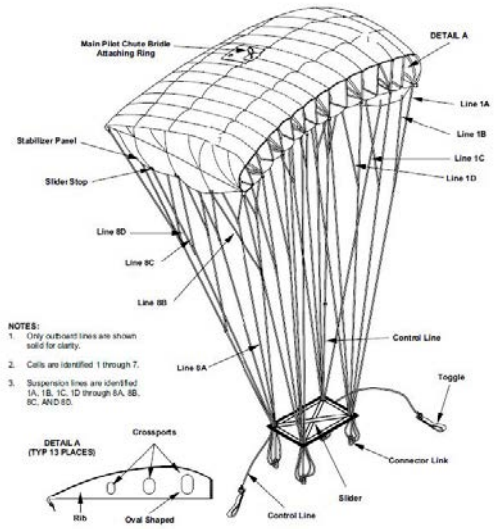

Fig. 2 Army MC-4/5 ram-air free-fall personal parachute system.

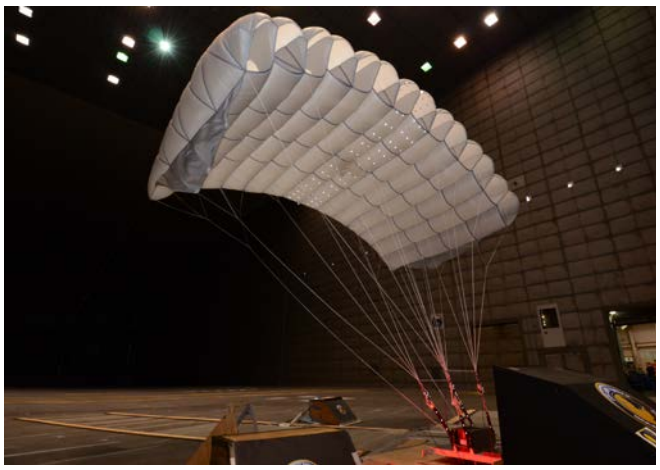

Fig. 3 Installation of ram-air parachute in test section.

by six 40-ft diameter fans, each driven by a motor rated at 23,000 Hp. These motors and fans also power the original 40- by 80-Foot test section of the closed-return circuit at airspeeds up to 300 kts.

IV. Test Articles

The test articles were canopies of the US Army MC-4/5 ram-air free-fall personnel parachute system (Fig. 2). These parachutes are designed for airdrops of personnel at weights up to 360 lbs. Each canopy is composed of 14 side-by-side segments that are open at the leading edge to allow ram-air inflation. The segments are separated by fabric ribs with the proprietary Lissaman 7808 airfoil shape. Suspension lines are attached to every second rib, and pairs of adjacent segments between suspension lines are defined as "cells." The span of the canopies, composed of seven cells, is 28.5 feet. The canopies are rectangular with a constant chord of 13 feet. Three canopies were tested: one that was brand-new (P61087) and two that had been previously used (SLX29266 and M4C13544).

The canopies flew approximately 20 feet above the floor of the test section (Fig. 3). They were attached by suspension lines, risers, and control lines to the AGU, a small-suitcase-size control box that was mounted to a platform just above the floor of the test section. Forces and moments on the platform were measured by a six-axis load cell mounted between the underside of the platform and a vertical post that was supported by the facility main strut carriage. The platform accommodated counter weights that were added as needed to offset pitching moments generated by the inflated canopy.

The suspension lines were gathered into four groups; each group was connected to a riser that was attached to one corner of the AGU. The risers consisted of linkages at their upper ends and straps at their lower ends where they were attached to the AGU. Each riser included a load cell. The lengths of risers could be adjusted manually between runs to alter the angle of attack of the canopy. Control lines extended from the trailing edges of the outboard cells to two motor-driven spools (port and starboard) in the AGU. The spools were used to reel the control lines in and out and thereby deflect the trailing edge of the canopy.

In the original test plan, the risers were not connected directly to the AGU. Instead, each riser was to be connected to a corner of a horizontal rectangular frame ("variable trim platform" or VTP) that was attached by short straps to the AGU. When the canopy was inflated, the VTP was

Fig. 4 Inflated canopy showing targets on centerline cell.

suspended above the AGU. The angle of the VTP, and thus of the canopy, could be remotely controlled by a trim control line which extended from the VTP to a third motor-driven spool in the AGU. Measuring the orientation of the VTP by photogrammetry was an important objective of the test, and a separate photogrammetry system was designed and deployed to accomplish this task. The VTP, however, was abandoned at the very beginning of the test because of difficulty in controlling the canopy with the VTP present [1]. Therefore, angle of attack was set manually by adjusting the lengths of the two upstream risers. Because significant effort was required to design and deploy the VTP photogrammetry system, we include a description of it in this paper; however, because the VTP was not used, we do not present any photogrammetry measurements from this system.

A plywood box, about 6-ft wide, 6-ft deep, and 4-ft high, was mounted on the floor just upstream of the AGU and shielded it from the free-stream flow. The box also provided a convenient shelter for an attendant who monitored the test article and made adjustments (e.g., added counter weights, adjusted risers) as necessary.

Adhesive retro-reflective targets were applied to the upper and lower surfaces of the central cell of the canopies (i.e., to half cells on either side of the centerline). The targets were two inches in diameter, 0.004 in thick, and were punched from 3M Scotchlite 7610 material [9]. They were arranged in seven equally spaced chord-wise rows that extended from the leading to the trailing edge of the canopy. On the lower surface there were 14 targets in each row (Fig. 4), and on the upper surface there were 17. The central row lay along the canopy centerline, i.e., along the central rib. The outermost rows were slightly inboard of the next outboard ribs. Targets were also applied to each of the four straps that connected the suspension lines to the AGU. All of the targets remained securely attached throughout the tests.

V. Instrumentation

A. Cameras and Lamps

The test articles were imaged by three sets of cameras. The first set consisted of three cameras that viewed the upper surface of the canopies from upstream, midstream, and downstream windows in the ceiling near the tunnel centerline (Fig. 5). These windows were accessible from the attic above the ceiling and were the only positions where cameras could be placed with good views of the canopy from above. The midstream and downstream cameras were Dalsa Falcon 2 12M (12 Mpixels) and the upstream camera was a Dalsa 4M15 (4 Mpixels). The third (upstream) camera was necessary to provide better visibility of the leading edge of the canopy. The convergence angle between the most upstream and downstream cameras was about 85°.

The second set of cameras consisted of two Dalsa Falcon 2 12M that imaged the lower surface of the canopy. Both cameras were mounted below the canopy on the floor of the test section, one on the tunnel centerline just upstream of the turntable, and the other was just downstream of the AGU and about five feet port of centerline. The off-centerline position of the downstream camera was required to avoid mounting to a grate in the floor. Otherwise, unlike the ceiling cameras, there was great freedom in placing these cameras. The convergence angle between their optical axes was about 56°. This was significantly less than the optimum angle of 90° but was necessary to avoid extremely oblique views of the canopy surface. Both cameras were shielded from the airflow by plywood shrouds.

The final set of cameras (two Dalsa 4M15) imaged the AGU straps from the starboard side. They were mounted on the floor, one approximately abeam the AGU and the other somewhat downstream (Fig. 6). Both cameras were shielded from the air stream by plywood shrouds. The downstream AGU camera viewed the test article through a sheet of Plexiglas that shielded it from the free-stream flow.

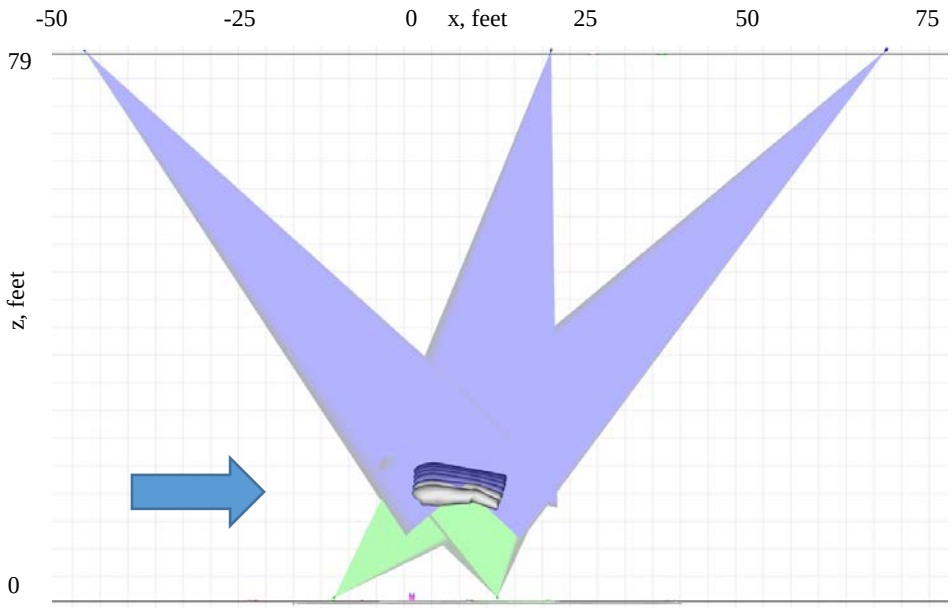

Fig. 5 Side view schematic of test section showing fields of view of ceiling (blue) and floor (green) cameras.

Placement, pointing, and choice of lenses for the cameras were planned well in advance of the test using virtual-imaging software [10, 11]. All of the cameras transmitted their images across Camera Link cables to IO Industries digital video recorders (DVRs, [12]). The distance from each camera to its DVR was longer than what Camera Link alone would allow. Therefore, these connections were extended using fiber optic cables with copper-to-fiber adapters at both ends. Breakout cables from all of the DVRs were connected by coaxial cables to a digital pulse generator (Stanford Research Systems DG-535) in the control room. All cameras began recording upon receiving a single TTL pulse from the DG-535, which was produced when the operator pressed the "single shot" button on the front panel of the DG-535. Since the test articles were assumed to be at steady conditions at most test points, the cameras were not precisely synchronized with the tunnel data acquisition system. Images from all three sets of cameras were displayed in real time on monitors in the control room. At most test points, data from all cameras were acquired at 15 Hz for two seconds at the beginning of each test point, which in most cases lasted two minutes. Images from all of the DVRs were downloaded to the computers and converted from IO Industries raw to TIFF format at the end of each shift.

A single, high-intensity white LED flash lamp was mounted next to each canopy camera (Fig. 7). An additional LED ring-lamp was added next to the downstream floor-canopy camera about halfway through the test to increase the brightness of the images. Both AGU cameras were fitted with red LED ring lamps (Fig. 6).

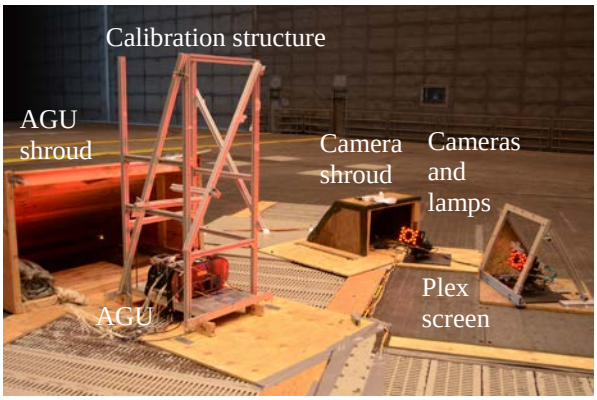

Fig. 6 Cameras and calibration structure for measuring targets on the AGU straps. Flow direction is top-left to bottom-right.

Fig. 7 Upstream floor-mounted canopy camera and lamp Flow direction is top-right to bottom-left.

1. Camera Calibration

Camera calibration involves finding coefficients of a transformation that maps points in 3D object-space to the 2D image plane of the camera. The floor and ceiling canopy cameras were calibrated using the collinearity equations, which assume a pinhole projection. Each ray from a point in object space (x, y, z) passes through the pinhole and is mapped to the image plane (X, Y) of the camera:

$$X = X_P - c_x \left[\frac{m_{11}(x - x_c) + m_{12}(y - y_c) + m_{13}(z - z_c)}{m_{31}(x - x_c) + m_{32}(y - y_c) + m_{33}(z - z_c)}\right]$$

$$Y = Y_P - c_y \left[\frac{m_{21}(x - x_c) + m_{22}(y - y_c) + m_{23}(z - z_c)}{m_{31}(x - x_c) + m_{32}(y - y_c) + m_{33}(z - z_c)}\right] \quad (1)$$

where (X_P, Y_P) is the principal point (where the optical axis passes through the image); (c_x, c_y) are respectively the horizontal and vertical image scale factors (proportional to focal length); (x_c, y_c, z_c) is the perspective center (camera position); and m_{ij} is a 3x3 rotation matrix whose elements are functions of the three camera point angles. (X, Y) are image-plane coordinates after correction for lens distortion. They are computed from measured coordinates (X_d, Y_d) by:

$$X = X_d - K_1(X - X_P)r^2 - K_2(X - X_P)r^4$$

$$Y = Y_d - K_1(Y - Y_P)r^2 - K_2(Y - Y_P)r^4 \quad (2)$$

where $r^2 = (X - X_P)^2 + (Y - Y_P)^2$and K_1 and K_2 are lens distortion correction factors. Taken together, (X_P, Y_P), (c_x, c_y), and (K_1, K_2) are the internal orientation of the camera; and (x_c, y_c, z_c) and m_{ij} are the external orientation or pose. Each camera was calibrated in two steps: first the internal orientation was measured, followed by the external orientation.

Before the internal orientation was measured, the cameras were positioned, pointed, and focused at the region of interest. Then, a sequence of images of a flat target board was acquired where the board filled the field of view of the camera and where the board's orientation was different in each image. Using the method of Zhang [13], the internal orientation was computed from the image-plane coordinates of the targets in all images and the known spacing between targets. Our preferred procedure is to hold the target board in the region of interest so that the optical path is exactly the same for calibration as for data acquisition. In the present test, however, the region of interest was too large (13 x 13 feet) and inaccessible (20 feet above the floor) to permit this. Therefore, after each camera was pointed and focused at the region of interest, the lens was taped and the camera was re-pointed to where a 4- by 4-ft target board could be conveniently hand-held at a distance that filled the field of view. At this much closer distance the target-board was somewhat out of focus, but the depth-of-field was adequate to allow the targets to be located accurately in the images. Another factor that compromised the internal calibration of the ceiling cameras was that they viewed the region of interest through thin glass windows, whereas, when the cameras were re-pointed at the target board, they were not looking through the windows. We assumed that the small effect of the window glass was accounted for in the external orientation.

After images for the internal orientations were acquired, the cameras were pointed at the region of interest, locked in position, and an image was acquired by each that included targets that were well-distributed in the field of view and whose space coordinates were known. The image- and object-space coordinates of these targets and the internal orientation of the camera were used to compute each camera's external orientation. This is a nonlinear least-squares problem that was solved by the Levenberg-Marquardt algorithm [14] and requires a first estimate.

It was a simple matter to distribute calibration targets on the floor of the test section where they were visible to the downward-looking cameras in the ceiling. However, distributing targets in the fields of view of the upward-looking cameras and measuring their positions presented two significant challenges: first, where to place the targets, and second, how to measure their positions. Placing targets was a problem because the only surface that appeared in the fields of view of these cameras was the ceiling of the test section, which, at 79 feet above the floor, was inaccessible from below, even from a man lift. Fortunately, an array of light fixtures in the ceiling was accessible from the "attic" above the ceiling and the fixtures were well distributed in the images. Therefore, by taping a downward-facing retro-reflective target to the glass cover in one corner of each fixture, we created an array of 68 well-distributed targets that was visible from below.

The next challenge was to measure the spatial positions of these targets. V-STARS could not be used because V-STARS requires placement of many coded targets in between the targets to be measured, i.e., on the ceiling between

Fig. 8 Measuring ceiling calibration targets with a theodolite.

light fixtures, which was inaccessible. Therefore, as an alternative to V-STARS, we used a theodolite to measure the elevation and azimuth angles to each of the targets from two widely separated (43 ft) reference points ("monuments") on the floor of the test section (Fig. 8). The positions of the monuments were precisely known from previous surveys using V-STARS. For each target, the theodolite measurements defined two lines in space (rays) that, for perfect measurements, would intersect at the target. In practice, the rays never intersected, and the target was assumed to lie at the point of closest approach between the rays, i.e., the midpoint of the unique line segment between the rays that is perpendicular to both. The length of this line segment (distance of closest approach) is an indication of the measurement uncertainty. For the 68 targets on the ceiling, the RMS of these distances was 0.43 inches. The theodolite was also used to measure the coordinates of 37 targets on the floor, where the RMS error was 0.63 inches. These uncertainties are much larger than the uncertainties of V-STARS measurements of calibration targets in previous tests (typically less than 0.005 inches). Many of the targets, particularly those in the ceiling light fixtures, were difficult to see through the theodolite telescope; and their centroids had to be judged by eye often while craning one's neck at very awkward angles.

Note that the calibration targets on the floor and ceiling were each coplanar. This precluded the use of the DLT, which requires out-of-plane targets, to calibrate the canopy cameras.

The AGU cameras were calibrated by placing an open structure made of extruded aluminum beams over the AGU (Fig. 6). Adhesive, retro-reflective targets were applied to the structure and their positions (relative to each other and the monuments) were precisely measured by V-STARS. The space and image-plane coordinates of these targets were used to compute a Direct Linear Transformation (DLT) for each camera.

B. Load Cells

All loads on the test articles were transferred to the six-axis load cell (Interface 6A68B, lift capacity = 899 lbs) below the platform to which the AGU was mounted [1]. In addition, S-type load cells (capacity = 500 lbs) were mounted in series with each of the four risers. Data from the load cells were recorded at one kHz by the tunnel data acquisition system.

VI. Data Reduction

Photogrammetry data were reduced using a Windows application ("Recession_2008") that was developed by the NASA Ames/AOX authors. This software implements methods from a wide variety of sources, including the "Photogrammetry Toolbox" developed by Liu and Burner [15]. Measurements can be made using images from up to 12 cameras, and the images do not all need to be of the same size. This was important in the present test because the upper surfaces of the canopies were measured by three cameras, two of which were significantly higher resolution (12 Mpixels) than the third (4 Mpixels).

A. Image Coordinates of Targets

The most tedious part of data reduction was locating targets in the images from all cameras. This was accomplished using an automatic target-finding function that searches for a target in a rectangular window centered on an estimated position of the target. The target finder first established a perimeter around each target and then computed the centroid of pixels within the perimeter. An ideal target can be located in this manner to better than about 0.1 pixels. The software includes functions that allow manually correcting the positions of incorrectly located targets.

The pattern of targets in the images from each camera remained approximately the same throughout the test. The main difference between images at different test points was a shift in the position of the pattern. This meant that once the targets had been located in a representative image, these locations could be used as starting points for automatically locating targets in images acquired at other test conditions. This approach worked well for shifts smaller than the size

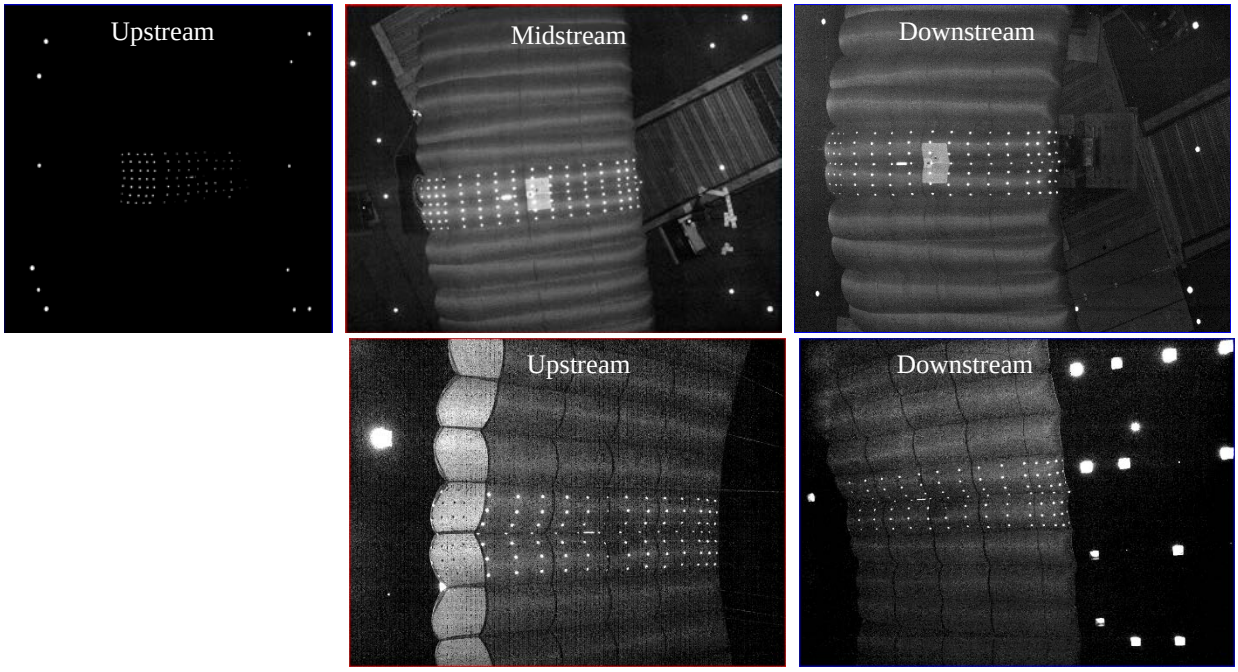

Fig. 9 Typical images from ceiling (top row) and floor (bottom row) canopy cameras. Flow is left to right.

of the search window. For larger shifts, a "group edit" function allowed the analyst to manually drag and drop the search windows for all targets as a group, whereupon the target finder automatically located the target in each re-positioned window.

B. Spatial Coordinates of Targets

Measurements of the upper and lower surfaces of the canopies were entirely independent of each other. The upper and lower surfaces were measured using only the ceiling and floor cameras, respectively. Moreover, the ceiling and floor cameras had no calibration targets in common.

The spatial coordinates (x, y, z) of each upper-surface target were computed from the pixel coordinates (X, Y) of the target in the images of the three ceiling cameras (A, B, C)[15]:

$$\begin{bmatrix} a_1^A & a_2^A & a_3^A \\ a_4^A & a_5^A & a_6^A \\ a_1^B & a_2^B & a_3^B \\ a_4^B & a_5^B & a_6^B \\ a_1^C & a_2^C & a_3^C \\ a_4^C & a_5^C & a_6^C \end{bmatrix} \times \begin{bmatrix} x \\ y \\ z \end{bmatrix} = \begin{bmatrix} a_1^A x_c^A + a_2^A y_c^A + a_3^A z_c^A \\ a_4^A x_c^A + a_5^A y_c^A + a_6^A z_c^A \\ a_1^B x_c^B + a_2^B y_c^B + a_3^B z_c^B \\ a_4^B x_c^B + a_5^B y_c^B + a_6^B z_c^B \\ a_1^C x_c^C + a_2^C y_c^C + a_3^C z_c^C \\ a_4^C x_c^C + a_5^C y_c^C + a_6^C z_c^C \end{bmatrix} \tag{3}$$

where

$$\begin{aligned} a_1 &= (X - X_P)m_{31} + c_x m_{11} \\ a_2 &= (X - X_P)m_{32} + c_x m_{12} \\ a_3 &= (X - X_P)m_{33} + c_x m_{13} \\ a_4 &= (Y - Y_P)m_{31} + c_y m_{21} \\ a_5 &= (Y - Y_P)m_{32} + c_y m_{22} \\ a_6 &= (Y - Y_P)m_{33} + c_y m_{23} \end{aligned}$$

The pixel coordinates (X, Y) were corrected for first- and second-order symmetrical lens distortion, Eq. (2). Equation (3) is an over-determined set of linear equations that was solved in a least-squares sense for (x, y, z). The same equation, but without the last two rows (corresponding to the third camera), was used to compute the space coordinates of each target on the lower surface. The spatial coordinates of all points on each surface were written to files in Tecplot format.

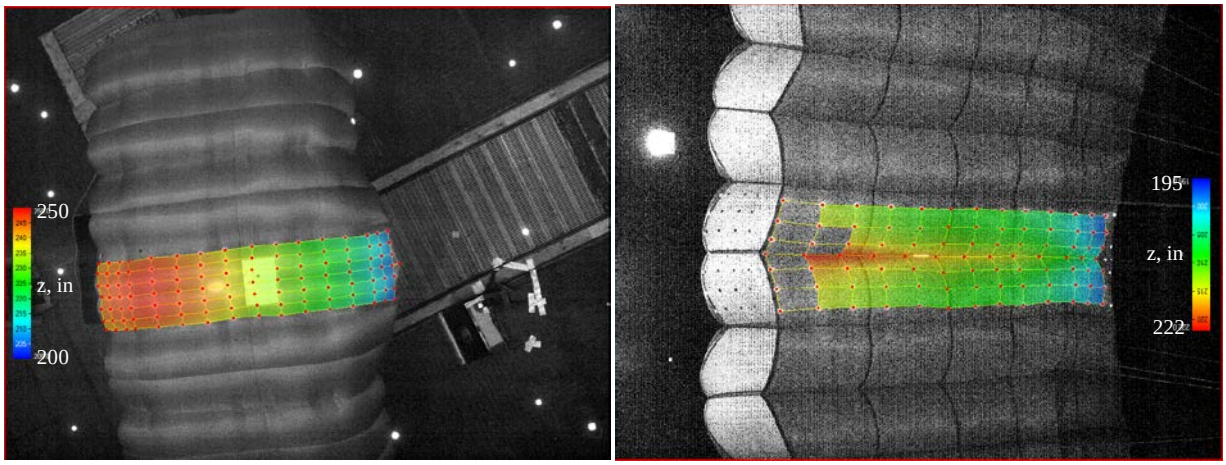

Fig. 10 Images of upper (left) and lower (right) surfaces of canopy with data overlay of z coordinates.

The solution to Eq. (3) is approximate, and each measurement includes an estimate of the measurement uncertainty. The standard deviation of each component of the least-squares solution (σ_x, σ_y, σ_z) can be estimated from the residual, i.e., the difference between the left- and right-hand sides of Eq. (3) (see Ref. [2], pp. 513-14 and Ref. [15], p. 81). Another way to quantify the uncertainty is to substitute (x, y, z) into the collinearity equations, Eq. (1), of each camera and compare the resulting "re-projected" image coordinates to the measured coordinates (after correction for lens distortion). Large re-projection errors usually indicated an incorrectly located target in the image of one or more cameras.

C. Angle of Attack

Angle of attack at each test condition was computed relative to the orientation of the test article at a reference condition. At each test condition the 3D spatial coordinates of all targets on both the upper and lower surfaces, except those on the flap, were compared to the spatial coordinates of the same targets at the reference condition. A rigid-body transformation was computed that, when applied to the targets at the test condition, yielded the best fit to the coordinates of the targets at the reference condition. This is a non-linear least-squares problem that was solved by the Levenberg-Marquardt algorithm. This procedure made maximum use of the target information.

The absolute angle of attack at each reference condition was computed from a linear fit of z vs x data on the upper and lower surfaces along the centerline rib.

VII. Results

Test parameters were airspeed, trailing-edge flap deflection, and front riser length. The front riser lengths were always set manually before each run and remained fixed throughout the run. The downstream risers were never adjusted and were the same for all runs. The trailing-edge deflection was adjusted during each run by commanding the AGU to reel control lines in or out and was measured in inches of control line. The test attendant confirmed with a tape measure that the commanded control-line adjustments had been accomplished. The test attendant also added or removed counterweights as needed to prevent excessive rotation of the mounting plate.

The test program included three types of runs: a sequence of "endurance" runs, where the new canopy was tested at steady conditions for an accumulated test time of 10 hours; static parametric runs where the front-riser and flap deflection were parametrically adjusted at steady conditions; and dynamic flap-deflection runs where the flaps were adjusted during the measurement interval.

The dwell time at most conditions was two minutes; photogrammetry images from all cameras were acquired at 15 Hz for two seconds at the beginning of each test point. For "static" test points, where the flap deflection remained constant and the parachute was assumed to be stationary, the photogrammetry measurements were based on the instantaneous target locations in the first image from each camera.

Typical photogrammetry data are shown in Figs. 9–11. Figure 9 shows images from each of the upper- and lower-surface cameras. Contrast has been adjusted to allow both the targets and the canopy to be visible (except in the image from the upstream ceiling camera in which only the targets are visible). In Figure 10, images of the upper and lower

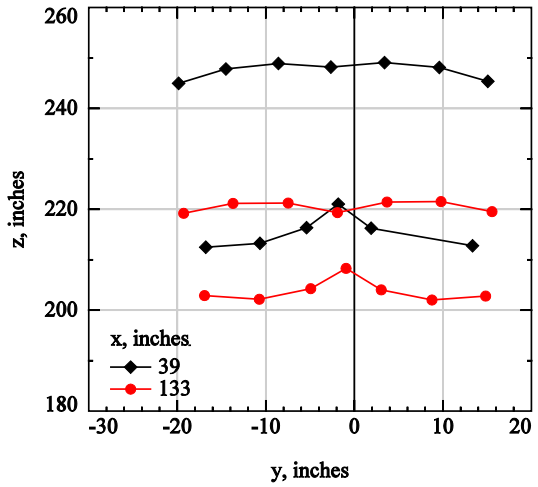

Fig. 11 Lateral shape of central cell: cross plot of z versus y at stream-wise stations near leading (black) and trailing (red) edges.

surfaces of the canopy have been overlaid by interpolated photogrammetry measurements of the vertical coordinate *z*. Targets at the leading and trailing edges of the canopies were not always visible to two cameras, so space coordinates at these points could not be computed when this occurred. Figure 11 shows cross-plots (*z* versus *y*) of these data at two stream-wise stations, one near the leading edge (black symbols), and the other near the trailing edge (red symbols).

A. Endurance Runs

The test began with a series of "endurance" runs of the brand new canopy (P61087). For these runs, the front risers were set to the same length as the rear risers (28.75 in), the flaps were not deflected, and the airspeed was constant (V = 29.2 kts). The cumulative test time of the canopy over seven runs was 600 minutes. During each run, photogrammetry data were acquired for two seconds every 5-10 minutes, and the tunnel was shut down every 30 minutes to allow the permeability of the fabric to be measured.

Figure 12 (a) shows the instantaneous angle of attack of the canopy at the beginning of each test point relative to the angle at the first test point (canopy P61087, flap = 0, riser = 28.75 in, V = 29.2 kts). Figure 12 (b) shows the lift coefficient, averaged over the duration of each test point. Both angle of attack and average lift coefficient increased very slightly as the flight time increased until the final sequence of 15 test points. Permeability measurements (which have not been released) showed very little change over the 10 hours of testing [1]. Before the final run (the last 15 test points) it was discovered that the front riser webbing had stretched about 0.5 inches, which would increase the angle of attack. Therefore, it is likely that the gradual increase in angle was due to a gradual lengthening of the front riser [1]. Before the final run (all test points after 60), the riser was reset to its original, shorter length, which explains the decreases in angle and lift coefficient. The angle of attack at the reference condition (first instance) was estimated to be 12.1° (Fig. 12, c).

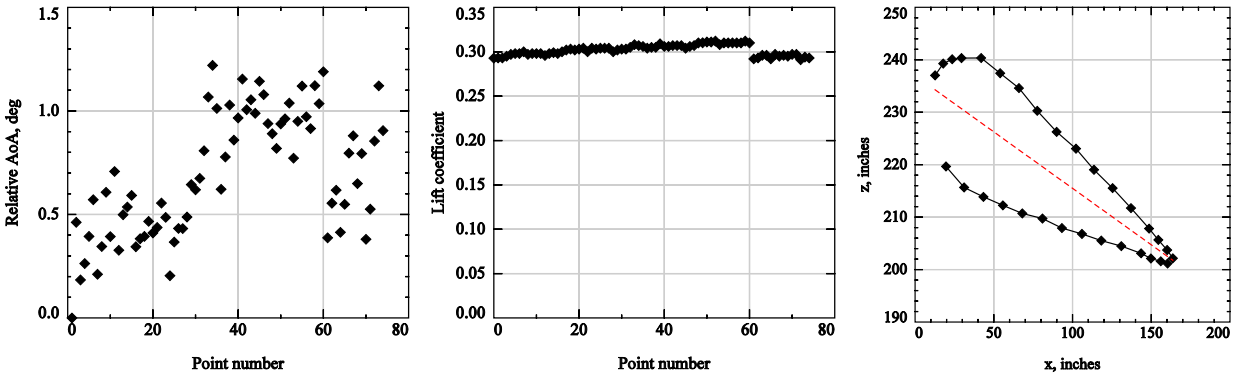

Fig. 12 Endurance runs: a) relative AoA vs point number; b) lift coefficient vs point number; c) *z* vs *x* along centerline at first point. Dashed red line is least-squares linear fit (α_{ref} = 12.1°).

B. Effects of Front Riser Length and Trailing-Edge Flap Deflection

Following the endurance runs, each canopy was tested over a range of front riser settings where, during each run, the flaps were deflected in equal increments between 0 and 30 inches. The first of these flap-deflection runs was with the front risers set to the same (or nearly the same) lengths as the rear risers. For these runs the flap-deflection increment was 5 inches, and the flap sweep was repeated at three airspeeds (V = 19.4, 24.3, and 29.2 kts). Subsequent

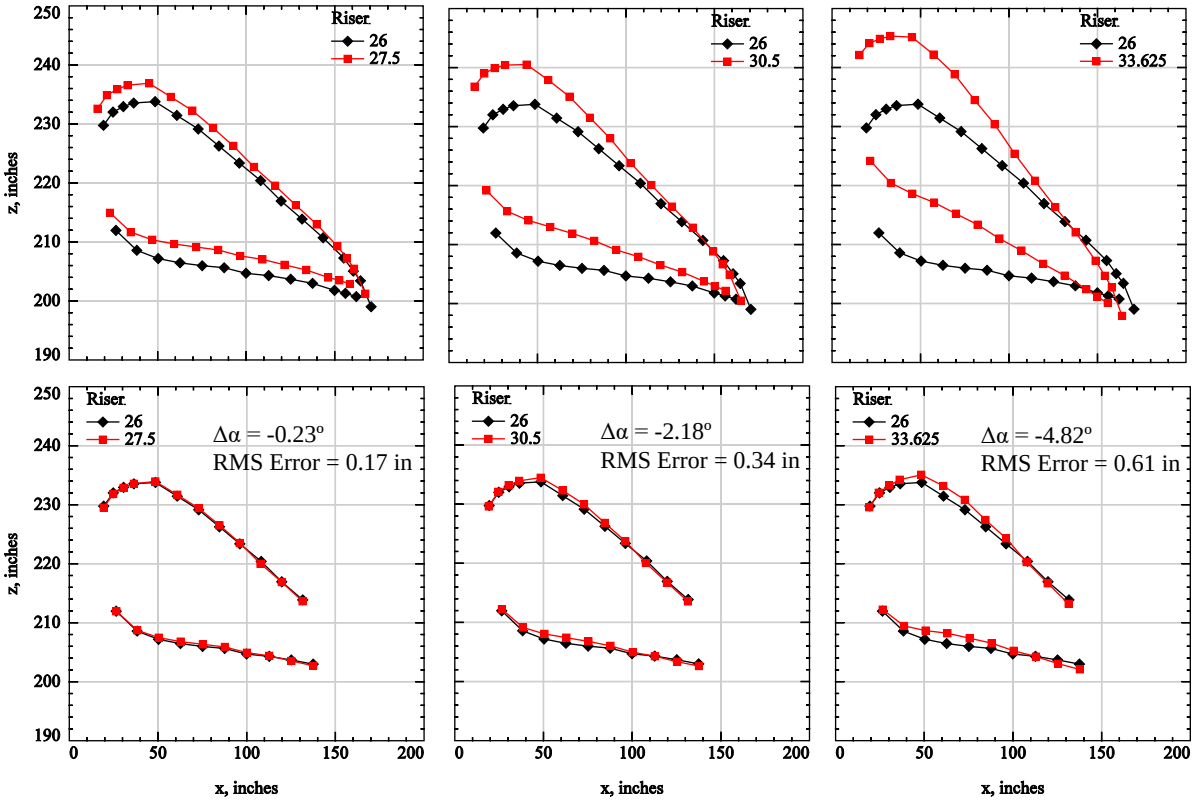

Fig. 13 Effect of front riser length on centerline target coordinates: raw data (top row); after rigid-body transformation (bottom row)(SLX29266; flaps = 0; V = 24.3 kts; α_{ref} = 8.78°)

flap-deflection runs, each with a different front-riser setting, were conducted at fewer conditions: at only one airspeed (V = 24.3 kts) and with flap-deflection increments of 10 inches.

Figure 13 (top row) shows how changing the length of the front riser affected the positions of the targets along the centerline of the upper and lower surfaces of the canopy (canopy SLX29266, flap = 0, V = 24.3 kts). Data at each riser setting are compared to data at the minimum setting (riser length = 26 inches). As expected, increasing the length of the riser caused the leading edge of the canopy to rise and the angle of attack to increase. Figure 13 (bottom row) compares measurements for the same cases after each was transformed as a rigid body to give the best fit to the measurements at the reference condition. The change in pitch angle and the RMS error of the fit are indicated for each case. These transformations significantly reduced differences between data at each riser setting and the reference condition. This supports the rationale for using these transformations to define the relative angle of attack. Note that Fig. 13 only shows data along the canopy centerline whereas the rigid-body transformations were computed using all targets, including those off centerline.

The effect of deflecting the trailing-edge flap on the positions of the centerline targets is shown in Fig. 14 (canopy SLX29266, front riser length = 26 inches, V = 24.3 kts). The trailing edge rises as flap angle increases, and angle of attack decreases. Coordinates that have been transformed as a rigid body to give the best fit to the coordinates at flap = 0 are shown in Fig. 14 (bottom). The transformations were computed using all targets except those on the flap (the five most downstream targets in each row). The transformed target coordinates are in reasonably good agreement with the coordinates at the reference (flap = 0) condition.

Lift and drag coefficients and lift-to-drag ratios are shown as functions of relative angle of attack in Fig. 15. The lift and drag coefficients are averages of load-cell data for the entire two-minute test point whereas the photogrammetry data are for instantaneous measurements at the beginning of the test point. At each flap setting, angle of attack and lift increased as the length of the front riser increased. For a fixed front-riser setting, deflecting the flaps decreased the angle of attack, but there was a net increase in lift due to the added lift of the flap. The lift-curve slope

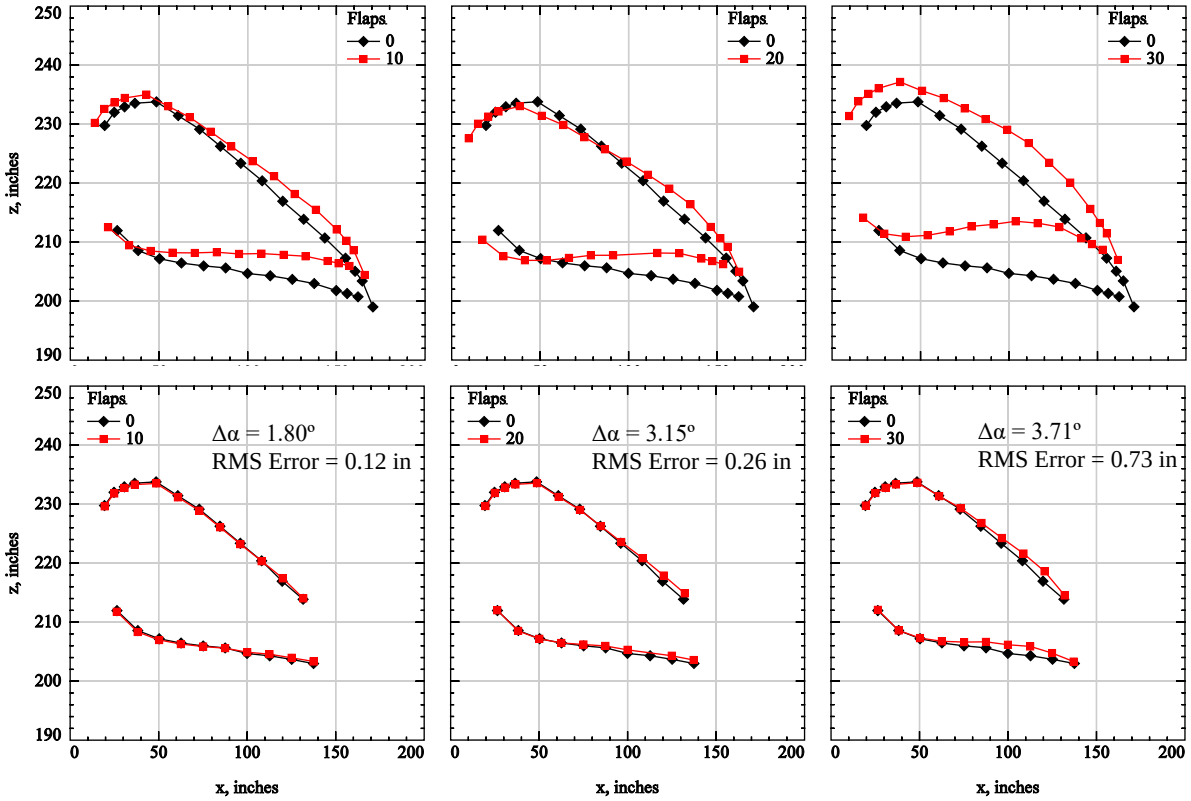

Fig. 14 Effect of flap deflection on centerline target coordinates: raw data (top); after rigid-body transformation (bottom)(SLX29266; riser = 26 inches; V = 24.3 kts; α_{ref} = 8.78°)

was approximately the same at all flap settings. For a fixed flap setting, drag increased slightly with angle of attack, and increased significantly as flap deflection was increased. Finally, the lift-to-drag ratio of each canopy increased with angle of attack and was nearly insensitive to flap setting. The highest relative angle, and thus the highest L / D, occurred at the maximum front riser length and no flap deflection.

C. Unsteadiness at Static Test Points

Much of the scatter in the photogrammetry data at static test points (Figs. 12 and 15) was likely due to low-frequency unsteadiness of the canopy. Figure 16 shows instantaneous relative angle of attack measurements computed from the full two seconds of photogrammetry data for the first and last endurance test points. The data at both points clearly show a low-frequency unsteadiness. More than two seconds of data would be required to define a meaningful average.

D. Dynamic Trailing-Edge Flap Deflection

The test also included a series of test points where the trailing-edge flap was dynamically adjusted as photogrammetry and load-cell data were being acquired. These test points included cases where flap deflection was increased from an initial deflection of 0 to a final deflection of 10, 20, or 30 inches; cases where flap deflection was decreased from an initial deflection of 10, 20, or 30 inches to 0; and cases where flap deflection was first increased from 0 to 10, 20, or 30 inches and then returned to zero. For these test points, photogrammetry data were acquired at 15 Hz for the entire test interval—up to 30 seconds for the 0-30-0 inch cases (450 images per camera).

Figure 17 (left column) shows the time histories of relative angle of attack and lift coefficient computed from load-cell data for two 10-second test points where, in the first (shown in black), the trailing-edge flap deflection was increased from 0 to 30 inches, and in the second (red) the deflection was reduced from 30 to 0 inches (canopy P61087, front riser = 29 inches, V = 24.3 kts). The photogrammetry measurements were computed for all 150 instances in the 10-second interval. The time histories of the flap deflections were not recorded. Deflecting the flap reduced the angle of attack, but overall lift increased because the increase in lift due to the flap deflection exceeded the loss of lift at the

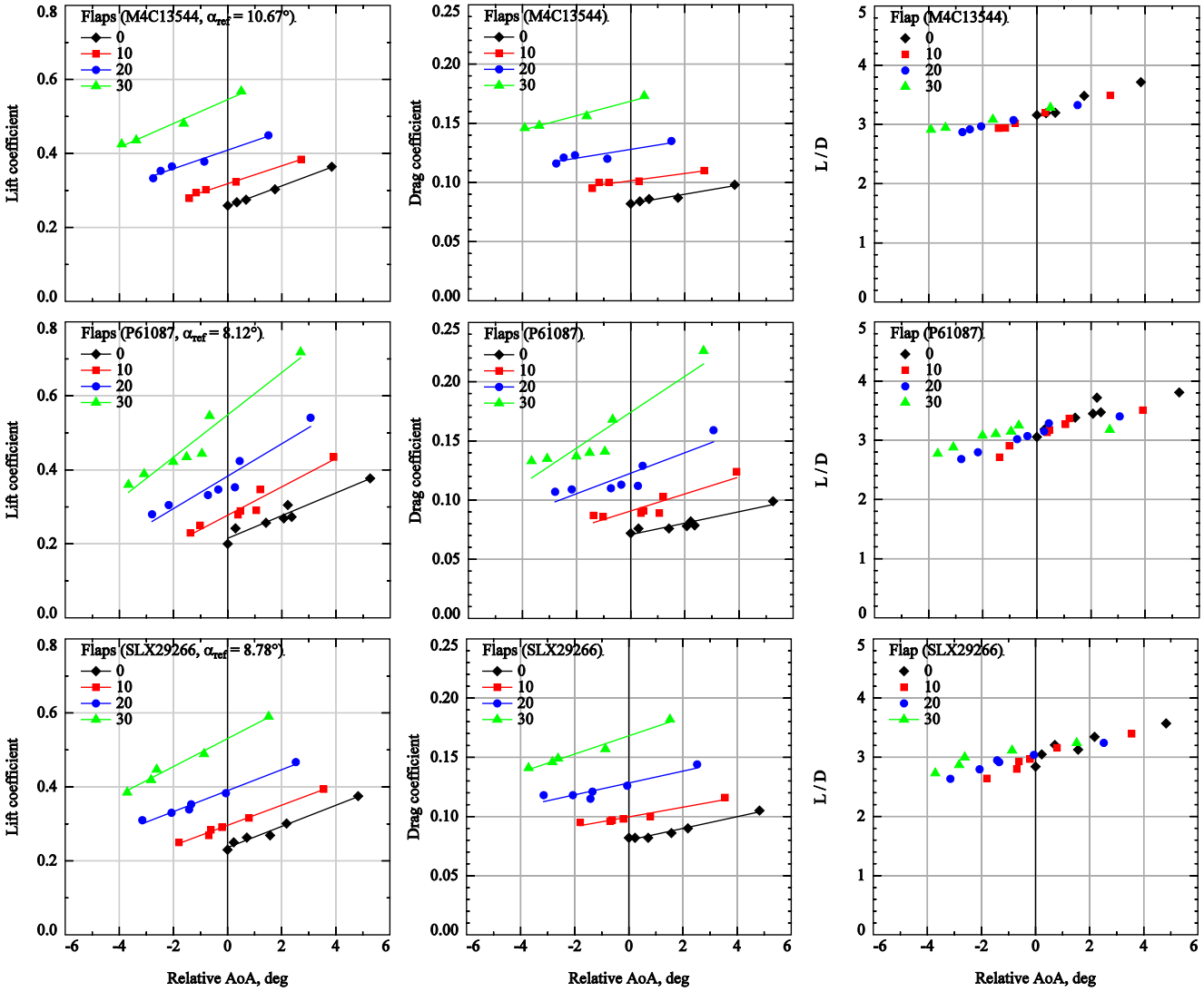

Fig. 15 Lift coefficient (left column), drag coefficient (center column), and L/D (right column) versus relative angle of attack for three canopies (V = 24.3 kts).

lower canopy angle. The inverse relationship between lift and flap deflection was also evident when the flap deflection was decreased. In both cases, the canopy attitude quickly stabilized after the dynamic flap deflection was complete.

Figure 17 (right column) shows time histories of relative angle of attack and lift coefficient for a 30-second test point where the flap was first increased from 0 to 30 inches and then decrease back to 0 (canopy P61087, front riser = 29 inches, V = 24.3 kts). For this longer point, only every other image from each camera was analyzed. As before, deflecting the flap produced a decrease in relative angle but a net increase in lift.

VIII. Uncertainties

Uncertainty of photogrammetry measurements depends on many factors including: on how accurately the camera calibrations map points from 3D object space to the 2D image plane; the number of cameras and their relative view angles; and how accurately the targets can be located in the images.

The methods used to calibrate the cameras were not ideal: for the internal orientation, the cameras were repointed at a target board that filled the fields of view but was much closer to the cameras than the region of interest. In addition, the internal orientations of the cameras in the ceiling did not include the window glass. Likewise, the external

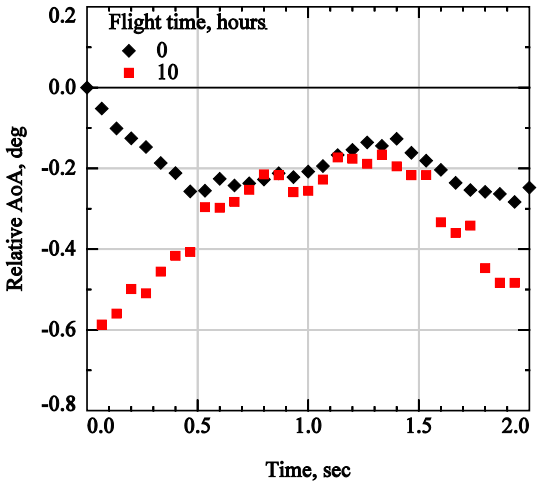

Fig. 16 Canopy unsteadiness: time histories of relative AoA during first (black) and last (red) endurance test points (P61087, riser = 28.75 inches, flap = 0, V = 29.3 kts, α_{ref} = 12.1°).

orientations were based on calibration targets whose spatial coordinates, measured with the theodolite, were not as precisely known as V-STARS measurements in previous tests. Nonetheless, the pinhole calibration of each floor and ceiling camera mapped the 3D object-space coordinates of the calibration targets to the camera's 2D image plane with an RMS difference of less than one pixel relative to the measured positions of the targets.

Even with a perfect calibration, there will be some error in computing spatial coordinates of a target due to uncertainty in locating the target in the images from all cameras. Target images were often far from ideal. Targets on the upper surface in images from the upstream ceiling camera were dim and elongated because of the very oblique view angle (Fig. 9). Targets on the lower surface in images from both floor-mounted canopy cameras were sometimes bisected by suspension lines. Targets along the centerline of both the upper and lower surfaces were in shallow crevasses formed by the adjacent inflated segments (e.g., Fig. 4), and their visibility was sensitive to small changes in the position and shape of the flexible canopy. It was common for several

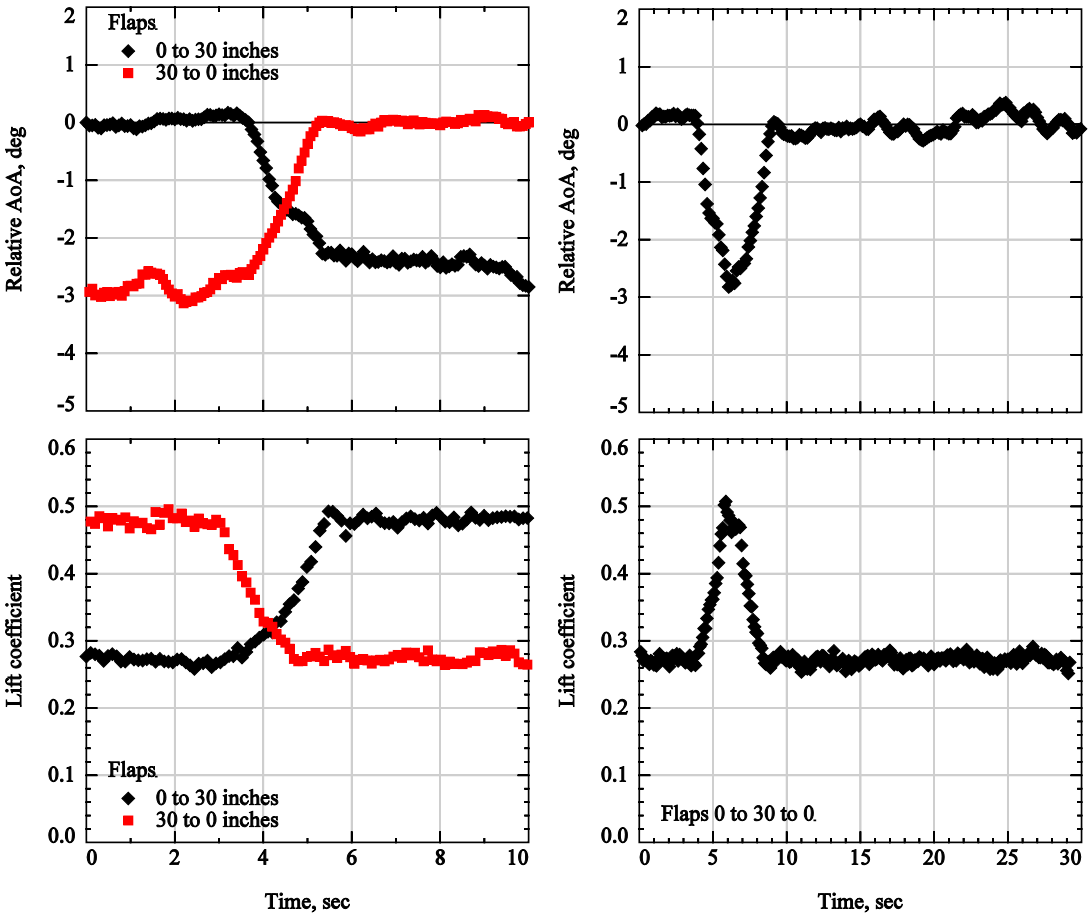

Fig. 17 Time histories of relative angle of attack (top row) and lift coefficient (bottom row) for dynamic flap deflections: at left, flap deflection is 0 to 30 (black) and 30 to 0 (red); at right, flap deflections is 0 to 30 to 0 (P61087, riser = 29 inches, V = 24.3 kts, α_{ref} = 10.91°).

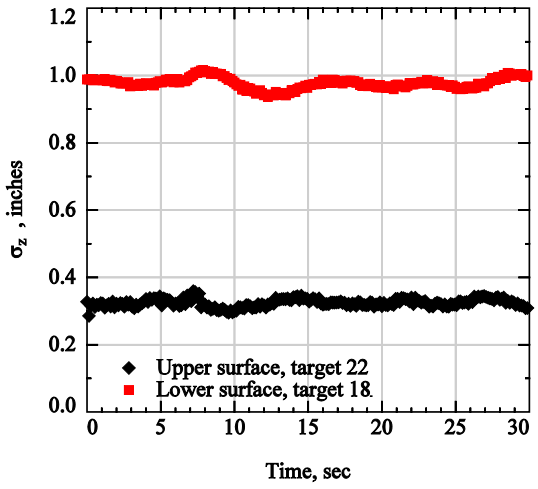

Fig. 18 σ_z versus time at targets on upper (black) and lower (red) surfaces during dynamic flap deflection 0-30-0 inches (P61087, riser = 29 inches, V = 24.3 kts, α_{ref} = 10.91°).

targets to be incorrectly located in each image, especially those from the upstream ceiling camera. These targets exhibited large re-projection errors and their positions were manually corrected by "point-and-click" on an enlarged view of the target.

The effect of random errors in locating the targets in the images was estimated by perturbing the image coordinates of a typical target in the image from each camera, one at a time, and computing the resulting change in the object-space coordinates. The square root of the sum of the square of these differences over images from all cameras yielded a measure of the overall sensitivity to uncertainty at that target. In the present tests, a random error of 1 pixel in locating targets (a very conservative estimate—well-defined targets can usually be located to within 0.1 pixels) corresponded to a change in the computed spatial coordinates of the target of less than 0.1 inch in each direction. This uncertainty was about the same for measurements from both the floor and ceiling cameras.

The propagation of random target-finding errors into the relative angle-of-attack measurements was estimated in a similar way. Each angle-of-attack measurement was a function of the pixel coordinates of all upper- and lower-surface targets (except those on the flap) in the images from the three upper- and two lower-surface cameras. Pixel coordinates of each target were perturbed, one at a time, in the image from each of the five cameras; the resulting change in angle of attack was computed and squared; the squared differences were summed over all targets and all images; and the square root of the sum was computed. For a typical case, a random error of 1 pixel in locating targets corresponded to a change in relative angle of attack of 0.02°. For small perturbations, this angle error, as well as errors in x, y, and z, scaled linearly with the magnitude of the target-finding errors.

The least-squares solution for (x, y, z) from Eq. (3) included estimates of the standard deviation of the measurement in each direction (σ_x , σ_y , σ_z). Figure 18 shows σ_z versus time for a typical target on the upper and lower surface of the canopy for the 30-second 0-30-0 dynamic flap-deflection case. The magnitude of σ_z at the lower-surface target (about 1 inch) is greater than at the upper surface target (about 0.3 inch). This difference may be due in part to the smaller and less optimal parallax angle between the lower cameras (56° vs 85°). In addition, images of the lower surface were significantly dimmer than those of the upper surface and viewing angles of the retro-reflective targets were more oblique. Finally, the downstream floor camera was located in a high-traffic area under the canopy where it was susceptible to tangling with suspension lines as the canopies were launched and recovered. Note that the standard deviations of measurements on both surfaces show periodicity that suggests systematic bias errors. Similar small periodic structure was evident in re-projection errors in the images of all cameras.

After the test, a structure with validation targets whose relative positions were precisely known was lifted into the volume occupied by the canopies (20 feet above the AGU), and images were acquired with the floor and ceiling canopy cameras. The spatial coordinates of targets visible to the floor and ceiling cameras were computed independently (none were visible to both the floor and ceiling cameras). The computed coordinates were then rotated and translated as a rigid body to give the best fit to the known spatial coordinates. After this transformation, the measured coordinates agreed with the known coordinates to within about 0.02 inches in each dimension.

The validation targets were also used to test the consistency of measurements from the floor and ceiling cameras. Although none of the these targets was visible to both the floor and ceiling cameras, the distances of targets visible only to the ceiling cameras from targets visible only to the floor cameras were known. In the vertical (z) direction, the distance between targets independently measured by the floor and ceiling cameras exceeded the known vertical distance by about 0.8 inches. In the stream-wise (x) direction, measurements from the ceiling cameras were offset downstream about 1.6 inches (1% chord) relative to measurements from the floor cameras, and in the lateral (y) direction, the offset was 0.7 inches (0.2% span). These small offsets had a negligible effect on the relative angles of attack computed from the target coordinates.

The above analyses suggest that most of the uncertainty in the photogrammetry measurements was due to bias rather than random errors and that this uncertainty was on the order of one inch in each direction. At the scale of the test article and the wind tunnel this is a small error, but improved accuracy is clearly possible.

IX. Concluding Remarks

Photogrammetry was successfully used to measure the shape and angle of attack of ram-air parachutes in the 80- by 120-ft test section of the NFAC. Three photogrammetry systems were deployed: one to measure the upper surface, one to measure the lower surface, and a third to measure the orientation of a "variable trim platform." Three canopies were tested at free-stream velocities of 19.4, 24.3, and 29.2 kts. In addition to airspeed, two parameters were varied: length of the front risers and the deflection of the trailing-edge flaps. Forces and moments on the parachutes were measured by a six-axis load cell. Together, the photogrammetry and load-cell data showed that increasing the front riser length at a fixed flap setting increased angle of attack and lift; and deflecting the trailing-edge flap at a fixed front-riser length reduced the angle of attack of the canopy but increased the net lift. Maximum lift-to-drag ratio occurred at the largest front riser setting and zero flap deflection, where angle of attack was greatest. Ten hours of testing of a new canopy at constant conditions showed small increases in angle of attack and lift with elapsed time. Photogrammetry measurements at most "static" test points were instantaneous and did not account for low-amplitude, low-frequency unsteadiness in the position and attitude of the canopies. Dynamic measurements, where the flap deflection was changed during the interval of the test point, showed strong inverse correlation between angle of attack and lift. The uncertainty in the photogrammetry measurements was approximately one inch in each direction. This uncertainty can likely be reduced by improving the camera calibration procedures.

Acknowledgments

This manuscript has been approved "DISTRIBUTION A. Approved for public release: distribution unlimited." by the U.S. Army Combat Capabilities Development Command, Soldier Center, PAO # U19-1137. The authors thank the staff of the NFAC who worked on this test, and, in particular, Charles Rogers who, at the time of the test, was US Air Force NFAC Test Engineer Group Lead.

References

[1] Ellerbee, J. and Sayles, E., "Natick Soldier Research Development Center (NSRDEC) Ram-Air Canopy," AEDC-TR-18-N-07, July 2018.
[2] Wolf, P.R., *Elements of Photogrammetry*, McGraw-Hill, New York, 1974.
[3] Meyn, L., and Bennett, M., "A Two Camera Video Imaging System with Application to Parafoil Angle of Attack Measurements," AIAA Paper 91-0673, presented at the 29th Aerospace Sciences Meeting, Jan. 7-10, 1991, Reno, NV.
[4] Matos, C., Mahalingam, R., Ottinger, G., Klapper, J., Funk, R., and Konerath, N.M., "Wind Tunnel Measurements of a Parafoil Geometry and Aerodynamics," AIAA Paper 98-0606 presented at the 36th Aerospace Sciences Meeting, Jan. 12-15, 1998, Reno, NV.
[5] Schairer, E.T., Kushner, L.K., Heineck, J.T., and Solis, E., "Measurements of Parachute Dynamics in the World's Largest Wind Tunnel by Stereo Photogrammetry," AIAA 2018-3802.
[6] URL: https://www.geodetic.co/v-stars/ [retrieved 15 March 2018].
[7] Abdel-Aziz, Y.I., and Karara, H.M, "Direct Linear Transformation from Comparator Coordinates into Object-Space Coordinates," Proceedings of the Symposium on Close-Range Photogrammetry, Urbana, IL, January 1971.
[8] URL: https://www.nasa.gov/centers/ames/news/features/2012/nfac-25html [retrieved 15 March 2018].
[9] URL: multimedia/wms/media/1047216O/3m-scotchlite-high-grain-reflective-sheeting-7610.pdf [retrieved 19 April 2019].
[10] Schairer, E.T., Heineck, J.T., Walker, S.M., and Yaste, D. M., "Predicting Camera Views for Image-Based Measurements in Wind Tunnels," AIAA Paper 2005-1349, presented at 43rd Aerospace Sciences Meeting and Exhibit, Reno, NV, Jan. 10–13, 2005.
[11] Kushner, L.K. and Schairer, E.T., "Planning Image-Based Measurements in Wind Tunnels by Virtual Imaging," AIAA Paper 2011-0930, presented at 49th AIAA Aerospace Sciences Meeting and Exhibit, Orlando, FL, Jan., 2011.
[12] URL: www.ioindustries.com/core.html [retrieved 23 April 2019].
[13] Zhang, Z., "Flexible Camera Calibration by Viewing a Plane from Unknown Orientations," presented at International Conference on Computer Vision, Corfu, Greece, Sept. 1999, pp. 666–673.
[14] Press, W.H., Flannery, B.P., Teukolsky, S.A., and Vetterling, W.T., *Numerical Recipes, The Art of Scientific Computing*, Cambridge University Press, Cambridge, 1986, pp. 523-528.
[15] Liu, T., and Burner, A.W., "Photogrammetry Toolbox Reference Manual," NASA CR-2014-218518, Sept., 2014.